

1 **Aquatic macrophytes in morphological and physiological responses to the**  
2 **nanobubble technology application for water restoration**

3 **Shuo Wang<sup>1</sup>, Yunsi Liu<sup>1</sup>, Tao Lyu<sup>2</sup>, Gang Pan<sup>3\*</sup>, Pan Li<sup>1,4\*</sup>**

4 *<sup>1</sup>School of Environmental Science and Engineering, Tongji University, 1239 Siping Road,*  
5 *Shanghai, PR China.*

6 *<sup>2</sup>Cranfield Water Science Institute, Cranfield University, College Road, Cranfield, Bedfordshire,*  
7 *MK43 0AL, UK*

8 *<sup>3</sup>Integrated Water-Energy-Food Facility (iWEF), School of Animal, Rural, and Environmental*  
9 *Sciences, Nottingham Trent University, Nottinghamshire NG25 0QF, UK*

10 *<sup>4</sup>School of Environmental Science and Engineering, State Key Laboratory of Control and*  
11 *Resource Reuse, Tongji University, 1239 Siping Road, Shanghai, PR China.*

12 **Abstract**

13 Nanobubble technology, as an emerging and sustainable approach, has been used for remediation  
14 of eutrophication. However, the influence of nanobubbles on the restoration of aquatic vegetation  
15 and the mechanisms are unclear. In this study, the effect of nanobubbles at different  
16 concentrations on the growth of *Iris pseudacorus* (*Iris*) and *Echinodorus amazonicus*  
17 (*Echinodorus*) was investigated. The results demonstrated that nanobubbles can enhance the  
18 delivery of oxygen to plants, while appropriate nanobubble levels will promote plant growth,  
19 excess nanobubbles could inhibit plant growth and photosynthesis. The nanobubble  
20 concentration thresholds for this switch from growth promotion to growth inhibition were  
21  $3.45 \times 10^7$  and  $1.23 \times 10^7$  particles/mL for *Iris* and *Echinodorus*, respectively. Below the threshold,  
22 an increase in nanobubble concentration enhanced plant aerobic respiration and ROS generations  
23 in plants, resulting in superior plant growth. However, above the threshold, high nanobubble  
24 concentrations induced hyperoxia stress, particularly in submergent plants, which result in  
25 collapse of the antioxidant system and the inhibition of plant physiological activity. The

26 expression of genes involved in modulating redox potential and the oxidative stress response, as  
27 well as the generation of relevant hormones, were also altered. Overall, this study provides an  
28 evidence-based strategy to guide the future application of nanobubble technology for sustainable  
29 management of natural waters.

30 **Keywords:** Eutrophication control; Oxidant/antioxidant species; Chlorophyll content; Gene  
31 expression; Hormone generation

### 32 **Synopsis**

33 Our study provided an evidence-based strategy to guide the future application of nanobubble  
34 technology for sustainable management of natural waters.

## 35 **1. Introduction**

36 Nanobubbles are defined as bubbles with a diameter of less than 1000 nm with  
37 special characteristics resulting from their ultra-fine size<sup>1</sup>. Compare with the rapid and high  
38 gas transfer efficiency of microbubbles (bubble size in micrometres), the gas dissolution  
39 speed would be slower/more sustainable, e.g. increase the DO level in the water, for  
40 nanobubbles due to the longer lifetime and lower buoyancy. Additionally, the natural  
41 collapse of nanobubbles could generate reactive oxygen species (ROS), including hydroxyl  
42 radicals ( $\cdot\text{OH}$ ), superoxide radicals ( $\cdot\text{O}_2^-$ ), and singlet oxygen ( $^1\text{O}_2$ ).<sup>2</sup> Previous studies have  
43 also shown that micro/nanobubbles can improve the lysis of harmful algal cells and the  
44 detoxification of cyanotoxins.<sup>3</sup> Therefore, bulk micro/nanobubbles have been directly  
45 exploited to remove aerobically degradable pollutants (e.g., organic waste and ammonium)  
46 and harmful algal blooms (HABs) from eutrophic waters.<sup>4,5</sup> Alongside the use of bulk  
47 nanobubbles, a novel refinement of the technology, which involves interfacial nanobubbles,  
48 was developed in 2018, using natural minerals loaded with oxygen to deliver oxygen  
49 nanobubbles onto sediment surfaces.<sup>6,7</sup> This approach successfully reversed sediment  
50 hypoxia and reduced the flux of N and P from the sediment for over four months. Therefore,  
51 there has been increasing research interest and deployment on nanobubble technology for  
52 the in-situ control of eutrophication. Many companies in Asia, the US and Europe have  
53 become increasingly involved in projects that use nanobubble technology for HAB  
54 mitigation.<sup>3,8,9</sup> Nevertheless, both bulk and interfacial nanobubble treatments have mainly  
55 focused on the first step of water restoration, i.e. pollutant removal and sediment  
56 remediation. After the pollutants removal to a certain level along with the water quality  
57 improvement, the clear-water state in natural waters could offer a satisfactory situation for  
58 the restoration of aquatic vegetation in the later stage. Since the nanobubble technology

59 operation time and nanobubble concentrations have not been precisely regulated, the  
60 potential impact of nanobubbles on the later processes of aquatic vegetation growth and  
61 stabilisation is still unclear.

62 As an important part of the aquatic ecosystem, aquatic vegetation provides a variety  
63 of important ecological services, including improving water clarity, stabilising sediments  
64 and providing food and habitats for aquatic animals.<sup>10</sup> Unlike terrestrial plants, aquatic  
65 plants, particularly when fully submerged, are more likely to face problems of oxygen  
66 limitation. Reduced availability of oxygen for cell respiration is likely to limit energy  
67 production and negatively influence plant growth.<sup>11</sup> Nanobubbles, which have superior  
68 oxygen/air transfer efficiency, are expected to assist aquatic vegetation to overcome such  
69 oxygen shortages; indeed, they have been used to improve plant seed germination,<sup>12</sup>  
70 biomass growth (e.g., lettuce and spinach)<sup>13,14</sup> and crop yield (e.g., tomato)<sup>15</sup>. Moreover, it  
71 is reported that the nanobubbles in the water can stimulate endogenous ROS generation  
72 inside plants.<sup>16,17</sup> An appropriate ROS level is required to activate plant proliferative  
73 pathways,<sup>18</sup> and thus they can be considered to promote plant growth.<sup>16,17</sup> Therefore, it is  
74 hypothesised that the presence of the nanobubbles during the water restoration could not  
75 only remove the pollutants but also benefit the aquatic plants restoration.

76 However, as applied to water restoration, the parameters of nanobubble technology,  
77 such as the appropriate operation time and nanobubble concentrations, have not been  
78 precisely defined. This is important because excess oxygen and ROS levels are likely to  
79 result in oxidative damage that could overwhelm the plant's oxidative stress response and  
80 negatively impact its metabolism.<sup>19</sup> Indeed, intermittent micro/nanobubble aeration has  
81 been shown to cause oxidative damage to the root tip cells and thereby inhibit the growth of

82 spinach plants.<sup>20,21</sup> Liu et al (2016) also reported that the exogenous hydroxyl radicals ( $\cdot\text{OH}$ )  
83 resulting from high levels of nanobubbles in water decreased hypocotyl elongation and  
84 chlorophyll formation in carrot and spinach.<sup>16</sup> Furthermore, in our previous research, we  
85 found that the submergent plant, *Echinodorus amazonicus*, gained 25% less biomass in  
86 micro/nanobubble-aerated water compared with plants aerated by macrobubbles, even with  
87 similar dissolved oxygen (DO) levels.<sup>22</sup> Nevertheless, we hypothesise that the emergent  
88 aquatic plants, which dominate the vegetation of most shallow lakes and wetlands, may  
89 have a higher tolerance of nanobubbles as the majority of the plant biomass is above water  
90 level, but this has never been examined in detail. Therefore, a quantitative investigation of  
91 the effect of nanobubbles on the growth of both emergent and submergent aquatic plants  
92 will be crucial as a guide to the application of nanobubble technology to water restoration.  
93 It is further hypothesised that the plant physiological response, in terms of  
94 oxidant/antioxidant species generation, hormone production and gene expression, would be  
95 different for emergent and submergent aquatic plants.

96 In this study, *Iris pseudacorus* (*Iris*) and *E. amazonicus* (*Echinodorus*) were selected  
97 as examples of indigenous emergent and submergent aquatic vegetation, respectively. The  
98 sediment and water were collected from a light-eutrophic reservoir as a growth medium for  
99 both plant species, which were then subjected to different nanobubble concentrations ( $10^6$ -  
100  $10^8$  particles/mL). DO concentrations were kept at a similar level in plant cultures to  
101 investigate the effect of a single factor (i.e. nanobubble concentration). Plant morphology,  
102 e.g. biomass, root/leaf length and chlorophyll content, were monitored to evaluate the effect  
103 of nanobubbles on plant growth. We also assessed the characteristics of plant physiology,  
104 including oxidant/antioxidant species generation, gene expression patterns and hormone

105 production, to reveal the mechanisms of the plant response to nanobubble treatment.  
106 Overall, this study aimed to obtain the threshold nanobubble levels that support the growth  
107 of aquatic vegetation and provide evidence-based results to underpin the application of  
108 nanobubble technology to natural water restoration.

## 109 **2. Experimental Section**

### 110 **2.1 Aquatic plant preparation and in-situ collection of sediment and water**

111 Water and sediment/soil were collected from a light-eutrophic reservoir with surface  
112 area 2.7 km<sup>2</sup> and average water depth 3 m. The concentrations of total nitrogen and total  
113 phosphate in the water were around 1.05-2.27 and 0.06-0.16 mg/L, respectively. Algal  
114 blooms occur in the reservoir every summer with an algal density as high as 10<sup>7</sup> cells/mL.  
115 Nanobubble aeration was applied at the entrance of the reservoir, and subsequently  
116 combined with wetland areas. The sediment/soil samples were collected from the upstream  
117 of the reservoir, which located around 1.2 km from the entrance. *Iris* and *Echinodorus* are  
118 both prevalent native plants; seedlings of both species were bought from a local  
119 horticultural company (Rongyue Ltd., Shanghai, China). The initial height of the *Iris* was  
120 around 10 cm and the initial weight of the *Echinodorus* was around 20 g.

### 121 **2.2 Experimental setup and operation**

122 *Iris* and *Echinodorus* were cultivated at room temperature (25 ± 5°C) with a 10 h  
123 photoperiod per day (LED plant lamps, photosynthetic photon flux density 180 μmol m<sup>-2</sup> s<sup>-1</sup>,  
124 150D, GAKO, China). *Iris* was cultivated hydroponically to simulate the floating bed  
125 system and subsequent constructed wetlands in this reservoir, which was grown in a  
126 polymethyl methacrylate tank with dimensions 55 × 18 × 30 cm in groups of 16 seedlings.  
127 Emergent seedlings were inserted into the holes of a styrofoam plate floating on water and

128 cultivated for 21 days. *Echinodorus* was grown in polymethyl methacrylate cylinders with  
129 an inner diameter of 35 cm and a height of 40 cm. Each cylinder contained three plant  
130 clusters. Submergent seedlings were cultivated in sediment for 40 days. Surface water (20  
131 L) from the reservoir was used in each tank or column. All plants were stabilised for three  
132 days prior to the experiment.

133 The water condition was set to simulate the late stage of the nanobubble  
134 eutrophication remediation process. For both emergent and submergent plants, six parallel  
135 groups were prepared to investigate the effects of different nanobubble concentrations on  
136 plant growth. Each group had three replicates. The system without aeration treatment was  
137 set up as the control group. In the macrobubble (MAB) aeration group, normal air pump  
138 was conducted continuously. To achieve such different nanobubble concentrations, two  
139 most common methods, i.e. pressurisation and cyclone shear methods, were used in this  
140 experiment. It has been documented that there is no difference in the physicochemical  
141 properties of nanobubbles generated by the two methods except particle size and  
142 concentration<sup>20</sup>. The intermittent nanobubble aerations coupled with further dilution  
143 method were conducted in the nanobubble (NB) aeration groups (Table 1), which were  
144 categorized as low, medium, high and super-high NB groups according to different  
145 concentrations of nanobubble in the water.

### 146 **2.3 Nanobubble distribution and water quality measurement**

147 Each nanobubble aeration treatment was conducted in pure reservoir water with air as  
148 the gas source to simulate the experimental conditions before plant cultivation. Nanobubble  
149 size distribution (<1000 nm) from all groups were measured right after the intermittently  
150 aeration and/or dilution by dynamic light scattering using a NanoSight NS3000 instrument

151 (Malvern Panalytical, UK). Each measurement was replicated three times. During the  
 152 experiment, temperature, pH, DO levels of the water in all groups were measured every two  
 153 days using a YSI 556 multi-parameter system (Xylem Inc., USA). To avoid cross-  
 154 contamination, the probes were carefully cleaned with ultrapure water between  
 155 measurements.

156 **Table 1**

157 Experimental conditions and aeration methodologies in different groups.

Group	Aeration	Method and Instrument	Energy consumption
Control	No aeration	-	0
MAB	Continuously aeration	Air pump and porous diffuser (YTZ-312, YEE, 3W, China)	150 W/m <sup>3</sup>
L-NB	0.4 L water was taken out daily for 2-min aeration and replenishment	Pressurisation method (LF-1500, XINGHENG, 0.4L/min, 90W, China)	6.25 W/m <sup>3</sup>
M-NB	4 L water was taken out daily for 10-min aeration and replenishment	Pressurisation method (LF-1500, XINGHENG, 0.4L/min, 90W, China)	31.25 W/m <sup>3</sup>
H-NB	1-min aeration / 30 min	Cyclone shear method (Ubbled2.0, XINGHENG, 4 L/min, 100W, China)	166.67 W/m <sup>3</sup>
S-NB	1-min aeration / 30 min	Pressurisation method (MF-5000, XINGHENG, 4 L/min, 500W, China)	833.33 W/m <sup>3</sup>

158 MAB, L-NB, M-NB, H-MB, S-NB represent macrobubble aeration, low, medium, high and  
 159 super-high nanobubble aeration groups, respectively.

## 160 **2.4 Plant morphological and physiological responses**

### 161 **2.4.1 Plant growth**

162 At the end of the experiment, all plants were harvested and the fresh weight, root/leaf  
 163 length and chlorophyll content (HACH®, DR 6000, USA) were measured. The  
 164 transplanting-survival rates (the percentage of plants that was alive after 7 days) and  
 165 biomass growth ratios (the ratio of the final fresh weight divided by the initial fresh weight)



166 were calculated for the comparison between groups. Other measured parameters were based  
167 on the survived plants, which could avoid the bias of the initial stabilisation differences that  
168 wouldn't happen in the real application.

#### 169 **2.4.2 Oxidant and antioxidant species**

170 For each species of plant, 5 g tissue samples were taken randomly from leaves and  
171 roots; samples were mechanically homogenized in phosphate buffer at a mixing ratio of  
172 1:9 (w/v) on ice. The suspension was then centrifuged for 5 min at 12000 rpm at 4°C. In the  
173 presence of superoxide radical, hydroxylamine is oxidized to nitrite, which can be  
174 determined by adding 1 ml each of 17 mM sulphanilic acid and 7 mM 1-naphthalene acetic  
175 acid solutions to 1 ml reaction mixture. The components were mixed and after being left at  
176 room temperature for 20 min,  $A_{530}$  was measured to calculate the concentration of  
177 superoxide radical.<sup>23,24</sup>

178 The total antioxidant capacity (T-AOC) was measured with a T-AOC assay kit  
179 (colorimetric method, A015, Nanjing Jiancheng Bioengineering Institute). The buffer  
180 solutions, ABT solution, peroxide solution, Trolox solution and samples were then  
181 prepared according to the manual of the assay kit, and then the OD value of each tube was  
182 read using a Synergy™ HT Multi-Mode Microplate Reader at a wavelength of 405 nm. All  
183 measurements were performed in triplicate.

#### 184 **2.4.3 RNA sequencing analysis**

185 The transcriptome of the macrophytes from the MAB and nanobubble groups (at  
186 similar DO levels) was analysed after cultivation to obtain detailed expression profiles of  
187 genes involved in the response of the macrophytes to the growth conditions. The same  
188 amount tissues of three replications of each treatment were mixed together and used for

189 RNA-Seq experiments. The filtered differentially expressed genes (DEGs) were mapped to  
190 the GO database using Goseq<sup>25</sup> to obtain significantly enriched GO terms.

#### 191 **2.4.4 Plant hormones**

192 To understand the regulatory effect of plant hormones on plant growth and  
193 development, accurate and efficient measurements of individual plant hormones in leaves  
194 and roots are required. HPLC-ESI-MS/MS was used for quantitation of endogenous plant  
195 hormones, which included 3-indoleacetic acid (IAA), salicylic acid (SA), jasmonic acid (JA)  
196 and jasmonic acid-isoleucine (JA-ILE). For each species of plant, 5 g plant tissue  
197 samples were taken randomly from leaves and roots and separated tissues were frozen with  
198 liquid nitrogen, then lyophilized tissue samples were ground to a powder by high-speed  
199 agitation with ceramic beads for 5 s. Metabolites were extracted from ground tissues using  
200 acetonitrile-water (1:1, v/v) and then centrifuged for 10 min at 12000 rpm at 4°C. A portion  
201 (2 µL) of sample was loaded onto a HPLC system (AcQuity UPLC, Waters, USA)  
202 equipped with a 50\*2.1 mm Waters HSS T3 LC-MS column using a flow-rate of 2 µL /min  
203 and a binary solvent system comprising water with 0.1% (v/v) acetic acid (A) and  
204 acetonitrile with 0.1% (v/v) acetic acid (B) as mobile phases. The primary parameters of  
205 electrospray ionization mass spectrometry (Q exactive, Thermo, USA) were as follows:  
206 voltage: -2800V; temperature: 350°C; gas: nitrogen; nebulizing gas: 40 psi; auxiliary gas:  
207 10 psi. All measurements were performed in triplicate.

#### 208 **2.5 Statistical analysis**

209 The significance of differences in plant growth was analysed by one-way analysis of  
210 variance followed by Tukey's HSD test with  $p < 0.05$ . For RNA sequencing analysis, the  
211 read counts were adjusted with the edgeR program package using a one-scaling normalized

212 factor prior to differential gene expression analysis.<sup>26</sup> The p-value was adjusted using q-  
213 value, and the threshold for significantly different expression was set as “q-value<0.005 &  
214 |log<sub>2</sub> (foldchange) |>1”.<sup>27</sup> Origin 2018b (OriginLab, Northampton, MA, USA) was used for  
215 plotting.

### 216 **3. Results and Discussion**

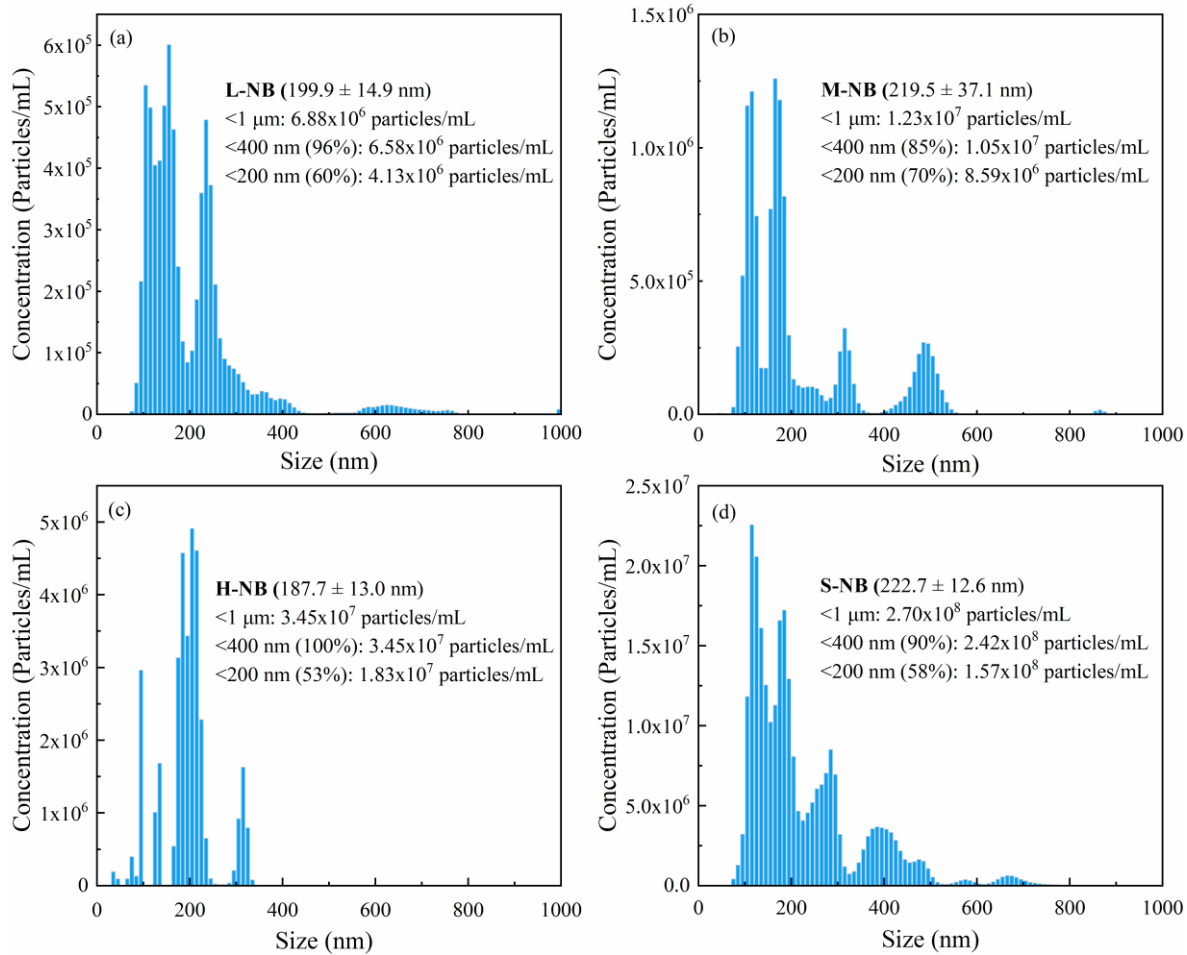
#### 217 **3.1 Nanobubble generation and DO level in water**

218 The mean particle sizes of the nanobubbles from the nanobubble aeration groups  
219 were similar and fell in to a range of 187.7-222.7 nm (Fig. 1). The concentration of  
220 nanobubbles (<1000 nm) was  $6.88 \times 10^6$  particles/mL in the L-NB group (Fig. 1a) and  
221  $1.23 \times 10^7$  particles/mL in the M-NB group (Fig. 1b). Higher nanobubble concentrations  
222 were observed in the H-NB and S-NB groups with  $3.45 \times 10^7$  and  $2.70 \times 10^8$  particles/mL,  
223 respectively (Fig. 1c and d). Notably, the control and macrobubble groups consistently  
224 contained  $<10^5$  particles/mL nanobubbles (data not shown). In the practical application,  
225 high concentrations of nanobubble (up to  $10^8$  particles/mL) could be formed in the water  
226 close to the nanobubble pump during the eutrophication remediation. However, the  
227 concentrations would be decreased along with the increased distance from the pump due to  
228 the dilution effect and nanobubble consumptions, e.g. oxidation with organic pollutants.  
229 Therefore, the whole range of the nanobubble concentrations, ranging from  $10^5$   
230 particles/mL (the background concentration) to  $10^8$  particles/mL, was conducted in this  
231 study to investigate the effect of the nanobubble on the aquatic plant growth.

232 Fig. S1 showed the difference of the DO levels in all groups, which was positively  
233 affected by the timing of nanobubble generation<sup>21</sup>. However, under current operations in  
234 this study, the DO levels in all groups fell into a relatively small range of 7.08-7.65 and

235 7.01-7.26 mg/L in *Iris* and *Echinodorus* cultures, respectively (Table 2). For both plants,  
236 similar DO levels were observed in control, L-NB and M-NB groups, with statistically  
237 lower values than those in other groups. The fluctuation of DO levels during the experiment  
238 was relatively greater in the emergent *Iris* groups than the submergent *Echinodorus* groups  
239 (Fig. S1). In addition, no significant difference in pH levels was observed among all *Iris*  
240 groups. However, pH level increased slightly along with the increased nanobubble  
241 concentration in the groups cultivated with *Echinodorus* (Fig. S2). Specifically, the average  
242 pH in the S-NB group ( $8.68 \pm 0.08$ ) was higher than that ( $8.41 \pm 0.14$ ) in the control group,  
243 which may be induced by the positive growth response of *Echinodorus* to the NB aeration  
244 (Fig. S2).

245         During aeration, the bubble size distribution affects the DO content in water, because  
246 bubbles of a smaller size have a proportionally greater surface area than large bubbles and  
247 can give a better oxygen transfer rate. However, perhaps controversially, in the current  
248 investigation nano-scale bubble aeration did not result in a very high DO level in water. It  
249 may be caused by the short-time operation of the nanobubble generation machine.’  
250 Moreover, previous studies have observed that nanobubbles are stable for days.<sup>28,29</sup> Atomic  
251 force microscopy (AFM) has also detected heterogeneous pressures inside nanobubbles,  
252 which was modelled in a molecular dynamics simulation as a high-gas-density state.<sup>30</sup> The  
253 oxygen inside nanobubbles may exist as an aggregation rather than the phase of dissolved  
254 oxygen, and the diffusion of the oxygen inside nanobubbles is likely to be slow and to take  
255 place over a long period of time. Thus, traditional instantaneous measurements of the DO  
256 level of water samples can detect the dissolved phase of oxygen, but may not fully reflect  
257 the total contribution of nanobubbles to any increase in gas transfer.



259

260 **Figure 1.** Nanobubble size distribution in L-NB (a), M-NB (b), H-NB (c) and S-NB (d)  
 261 groups. L-NB, M-NB, H-MB, S-NB represent low, medium, high and super-high  
 262 nanobubble concentration groups, respectively.

263 **Table 2**

264 The average DO levels in water during the cultivation of both aquatic plant species.

	Dissolved oxygen (mg/L)					
	Control	MAB	L-NB	M-NB	H-NB	S-NB
<i>Iris</i>	$7.08 \pm 0.50^b$	$7.49 \pm 0.56^{ab}$	$7.13 \pm 0.45^b$	$7.29 \pm 0.47^{ab}$	$7.52 \pm 0.65^{ab}$	$7.65 \pm 0.61^a$
<i>Echinodorus</i>	$7.01 \pm 0.25^b$	$7.21 \pm 0.19^{ab}$	$7.02 \pm 0.30^b$	$7.08 \pm 0.27^{ab}$	$7.26 \pm 0.18^a$	$7.23 \pm 0.19^{ab}$

265 MAB, L-NB, M-NB, H-MB, S-NB represent macrobubble aeration, low, medium, high and  
 266 super-high nanobubble concentration groups, respectively. Error bars indicate standard

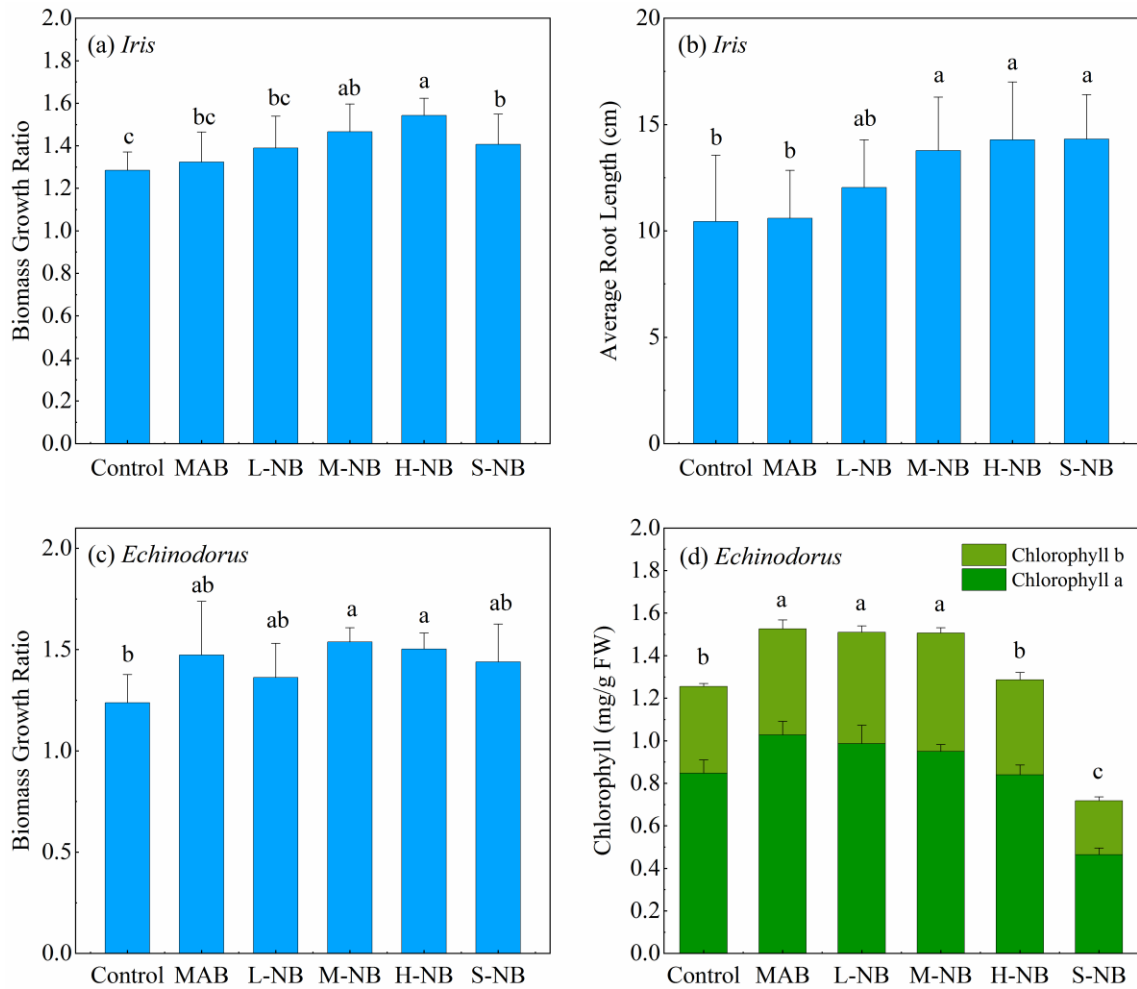
267 deviations. The superscript letters indicate significant differences ( $p < 0.05$ ) compared with  
268 other groups of the same plant.

### 269 **3.2 Plant morphology response to nanobubbles**

270 For *Iris*, the transplant-survival rates were 68.8%, 81.3% 81.3%, 93.8%, 100% and  
271 100% for the control, MAB, L-NB, M-NB, H-NB and S-NB groups, respectively. The  
272 biomass growth ratios were higher in all nanobubble treatment groups ( $1.39 \pm 0.15 - 1.54 \pm$   
273  $0.08$ ), followed by the macrobubble-aerated group ( $1.32 \pm 0.14$ ) and the control group ( $1.28$   
274  $\pm 0.09$ ) (Fig. 2a). In the nanobubble aeration groups, the plant biomass growth ratio  
275 increased along with increasing nanobubble concentration and reached the highest value of  
276  $1.54 \pm 0.08$  in the H-NB group (nanobubble concentration of  $3.45 \times 10^7$  particles/mL).  
277 However, after further increasing of the nanobubble concentration ( $2.70 \times 10^8$  particles/mL)  
278 in the S-NB group, the biomass growth ratio reduced to  $1.41 \pm 0.14$ , the significant  
279 difference were observed between H-NB and S-NB groups (Figure 2a,  $p < 0.05$ ). In  
280 summary, the plant biomass growth ratios in the MAB, L-NB, M-NB, H-NB and S-NB  
281 groups were 3%, 8%, 14%, 20% and 9.5% higher than that in the control group,  
282 respectively. The length of the *Iris* root followed a similar trend with average root lengths  
283 of  $12.04 \pm 2.24$ ,  $13.78 \pm 2.51$ ,  $14.29 \pm 2.71$  and  $14.31 \pm 2.09$  cm in the L-NB, M-NB, H-  
284 NB and S-NB groups (Fig. 2b and Fig. S3), compared with the macrobubble-aerated group  
285 ( $10.59 \pm 2.26$  cm) and the control group ( $10.44 \pm 3.12$  cm). No significant difference in leaf  
286 length or chlorophyll content between the various groups of *Iris* was observed, which may  
287 be due to the emergent plant leaf being out of the water and therefore less likely to be  
288 influenced by the nanobubbles in the water. The growth of the root, which is in direct  
289 contact with the nanobubbles, may be promoted by the increased aerobic respiration of the  
290 plant, which could cause new root formation.<sup>31–33</sup>

291           Regarding the submergent species, *Echinodorus*, the transplant survival rate was  
292 100%. The biomass growth ratios (around 1.5) in all macrobubble- and nanobubble-aerated  
293 groups were not significantly different (Fig. 2c). However, these values were generally  
294 significantly higher than that of the control group ( $1.24 \pm 0.14$ ). The length of both root and  
295 leaf in these groups followed the same trend. Although a similar biomass increase was  
296 observed in all aerated groups, some degradation of chlorophyll content and yellowing  
297 occurred in nanobubble-aerated groups (Fig. 2d), which is consistent with our previous  
298 study<sup>22</sup>. The threshold nanobubble concentration required to affect the chlorophyll content  
299 was identified in the M-NB group (1.51 mg/g FW). The excess nanobubbles present in the  
300 H-NB ( $3.45 \times 10^7$  particles/mL) and S-NB ( $2.70 \times 10^8$  particles/mL) groups drove the  
301 chlorophyll content significantly lower (1.29 and 0.72 mg/g FW, respectively), supporting  
302 the notion that photosynthesis is likely to be adversely affected by high concentrations of  
303 nanobubbles.

304           The submergent and emergent plants exhibited a different response to nanobubbles,  
305 with the emergent species seeming to have a higher tolerance, which may be due to the  
306 different spatial locations of plant parts and/or species-specific antioxidant capacity.<sup>22</sup>  
307 Nevertheless, it can be concluded that aquatic plant growth can benefit from exposure to  
308 certain concentrations of nanobubbles, but overdosing with nanobubbles can damage plant  
309 growth (biomass) and health (chlorophyll content).



310

311 **Figure 2.** Biomass growth ratio of *Iris* (a) and *Echinodorus* (c), average root length of *Iris*  
 312 (b), and chlorophyll content of *Echinodorus* (c) at the end of the experiment. MAB, L-NB,  
 313 M-NB, H-MB, S-NB represent macrobubble aeration, low, medium, high and super-high  
 314 nanobubble concentration groups, respectively. Error bars indicate standard deviations. The  
 315 different letters indicate significant differences ( $p < 0.05$ ) compared with other groups of  
 316 the same plant.

### 317 3.3 Effect of nanobubbles on plant physiology

#### 318 3.3.1 Reactive oxygen species (ROS) and total antioxidant capacity (T-AOC)

319 Besides changes in morphology, plants can also modify their physiology in response  
 320 to differences in environmental conditions, including in temperature, light and growth  
 321 media. A growth medium with a high level of  $\text{DO}^{34}$  and/or oxidising substances<sup>16,17</sup> is

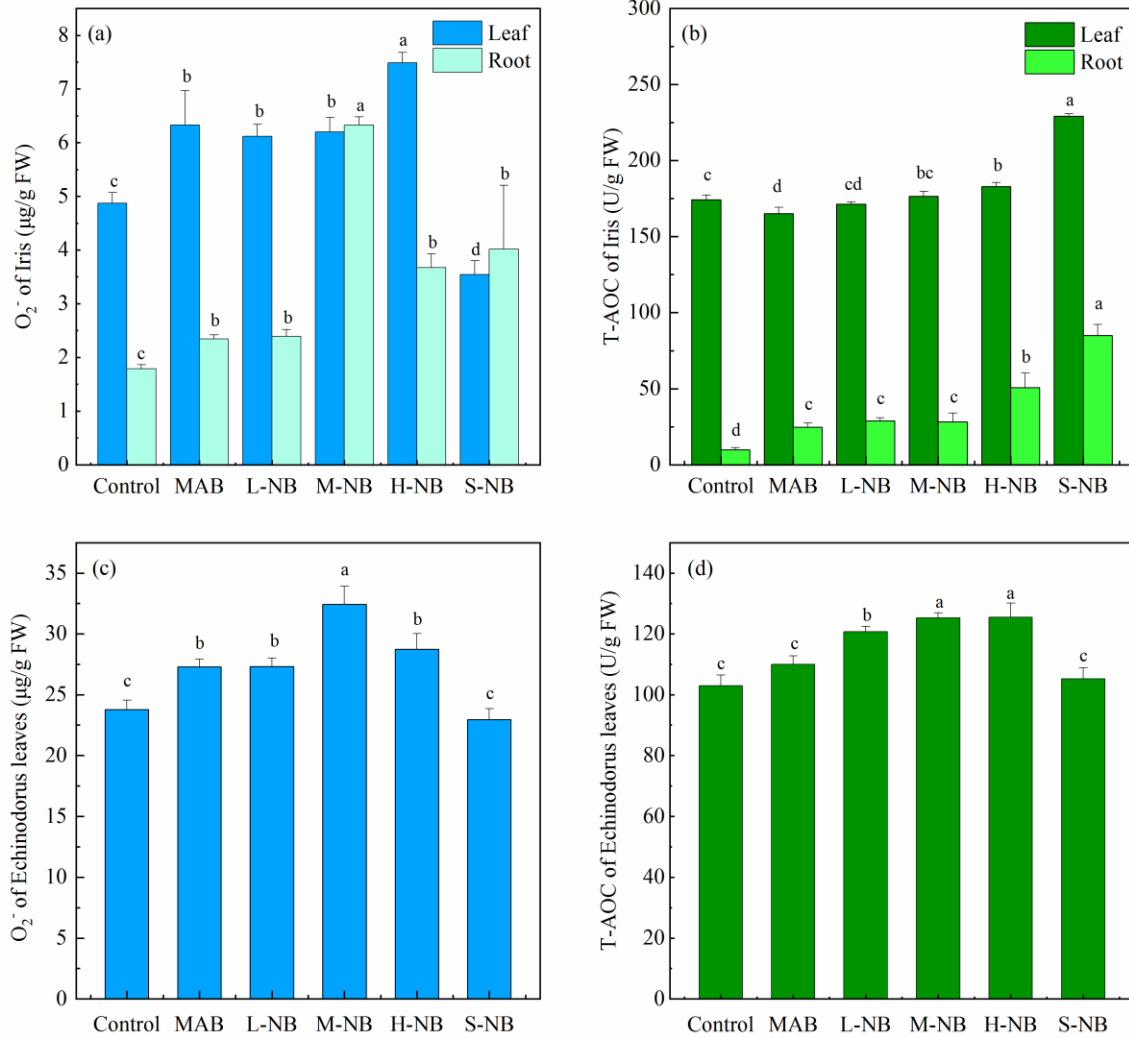


322 likely to stimulate endogenous ROS generation within plant tissues and thus to promote  
323 plant growth.<sup>18</sup> Accordingly, in the current investigation the concentrations of ROS  
324 (superoxide radical ( $\cdot\text{O}_2^-$ )) in *Iris* were significantly higher in MAB and nanobubble  
325 treatment groups (6.12-7.49 and 2.35-6.33  $\mu\text{g/g}$  FW in the leaf and root, respectively)  
326 compared with that (4.87 and 1.79  $\mu\text{g/g}$  FW in the leaf and root, respectively) in the control  
327 group (Fig. 3a), with the only exception being the S-NB group (3.55  $\mu\text{g/g}$  FW in the leaf).  
328 Notably, the highest ROS levels appeared in the H-NB group and then decreased at the  
329 higher nanobubble concentration in the S-NB group. This may be due to the increased  
330 levels of ROS accumulating within plants, which thereby induce oxidative stress. This is in  
331 line with the biomass results (Fig. 2a), where the highest *Iris* biomass was found in the H-  
332 NB group. In response to extremely oxidising conditions, the plant oxidative stress  
333 response will be stimulated, leading to an increase in total antioxidant capacity (T-AOC),  
334 which will act to maintain ROS at an appropriate level.<sup>19</sup> In root, the T-AOC increased  
335 consistently with nanobubble concentration from 9.79 U/g FW in the control group to  
336 around 26 U/g FW (MAB, L-NB and M-NB groups) and 50.79 U/g FW in the H-NB group,  
337 and reached the highest level (84.96 U/g FW) in the S-NB group (Fig. 3b). In the leaf, T-  
338 AOC content showed a similar trend and increased from approximately 170 U/g FW to 230  
339 U/g FW. The increase in ROS scavengers under highly oxidizing conditions<sup>18</sup> may explain  
340 the significantly lower ROS concentration in the S-NB plants compared to the H-NB group  
341 (Fig. 3a).

342 *Echinodorus* is expected to behave differently to the emergent species, *Iris*, because  
343 the whole plant grows under the water and thus has direct contact with nanobubbles.  
344 Because there was insufficient *Echinodorus* root for measurements, ROS and T-AOC

345 contents were only tested in leaves. The superoxide radical ( $\cdot\text{O}_2^-$ ) content in the leaf,  
346 compared to the control (23.76  $\mu\text{g/g}$  FW), increased in the macrobubble-aerated group  
347 (27.28  $\mu\text{g/g}$  FW), and increased with nanobubble concentration in the L-NB (27.32  $\mu\text{g/g}$   
348 FW) and M-NB (32.42  $\mu\text{g/g}$  FW) groups. However, the content then decreased to 28.73  
349  $\mu\text{g/g}$  FW and 22.95  $\mu\text{g/g}$  FW in the H-NB and S-NB groups, respectively (Fig. 3c). The  
350 same trend was also observed for T-AOC content in the leaves, but with the highest value  
351 (125.51 U/g FW) in the H-NB group, decreasing to 105.23 U/g FW in S-NB plants (Fig.  
352 3d).

353 Thus, because DO levels were similar in the MAB and nanobubble groups, the above  
354 effect on plant oxidant and antioxidant levels is probably due to the presence of  
355 nanobubbles. A previous study reported a consistent increase in antioxidant enzyme activity  
356 in soybean after 48 h exposure to increased oxidative stress,<sup>35</sup> consistent with our present  
357 findings. While oxygen promotes plant growth, this may become hyperoxia stress when the  
358 concentration of nanobubbles in the water exceeds  $3.45 \times 10^7$  and  $1.23 \times 10^7$  particles/mL for  
359 *Iris* and *Echinodorus*, respectively. It is worth noting that the thresholds for other plants  
360 may be different due to species-specific antioxidant capacities for each plant.<sup>22</sup>



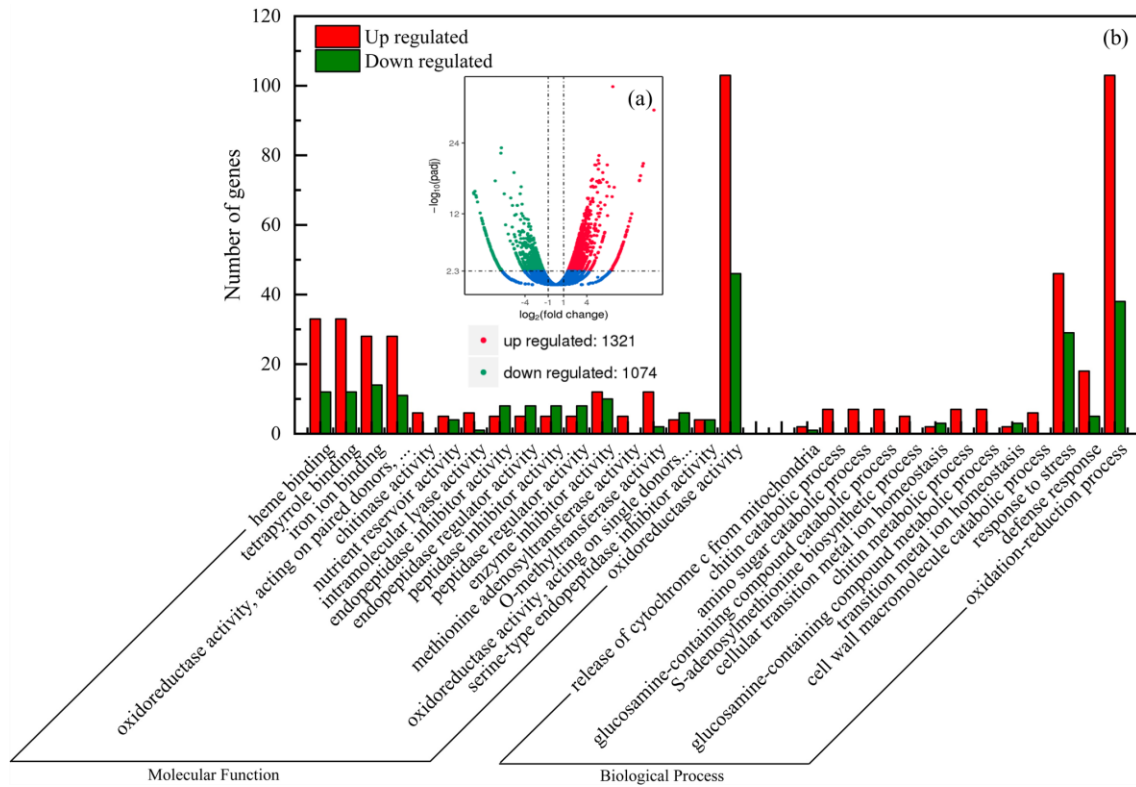
361

362 **Figure 3.** Superoxide radical concentration (a) and total antioxidant capacity (T-AOC) (b)  
 363 in the leaf and root of *Iris*; superoxide radical concentration (c) and T-AOC (d) in the leaf  
 364 of *Echinodorus* at the end of the experiment. MAB, L-NB, M-NB, H-MB and S-NB  
 365 represent macrobubble aeration, low, medium, high and super-high nanobubble  
 366 concentration groups, respectively. Error bars indicate standard deviations. The different  
 367 letters indicate significant differences ( $p < 0.05$ ) compared with other groups of the same  
 368 plant.

### 369 3.3.2 Transcriptional response

370 Based on the effects on plant morphology, *Iris* from the MAB and H-NB groups, and  
 371 *Echinodorus* from the MAB and S-NB groups, were selected to identify differentially

372 expressed genes (DEGs) that respond to nanobubble and macrobubble treatment at similar  
373 DO levels. In total, 1321 upregulated and 1074 downregulated unigenes were identified  
374 from *Iris* in the H-NB group, compared to MAB plants (Fig. 4a). The molecular functions  
375 of these genes are indicated by the associated GO terms, and several that were significantly  
376 enriched in *Iris* plants relate to oxygen binding, transfer and reduction (Fig. 4b). Plants use  
377 hemoglobins to bind and transfer oxygen efficiently,<sup>36</sup> which is then used for respiration.  
378 The upregulation of genes related to “heme binding”, “tetrapyrrole binding” and “iron ion  
379 binding” points to an enhanced ability to use oxygen in nanobubble-treated plants. In  
380 addition, the term “oxidoreductase activity, acting on paired donors, with incorporation or  
381 reduction of molecular oxygen” was also enriched, which indicates that the plants have  
382 received excessive molecular oxygen, leading to the genes involved in the reduction of  
383 molecular oxygen being overrepresented. The enhancement of oxygen delivery to plants  
384 induces ROS production (Fig. 3a), consistent with a group of 141 genes under the  
385 “oxidation-reduction process” umbrella being the most dominant group in the biological  
386 processes category; of these, 103 were upregulated unigenes and 38 were downregulated  
387 (Fig. 4b, Table S1). In addition, most genes related to “defense response” and “response to  
388 stress” in the biological process category were also upregulated, implying that the  
389 nanobubbles induce hyperoxia stress (Fig. 4b).



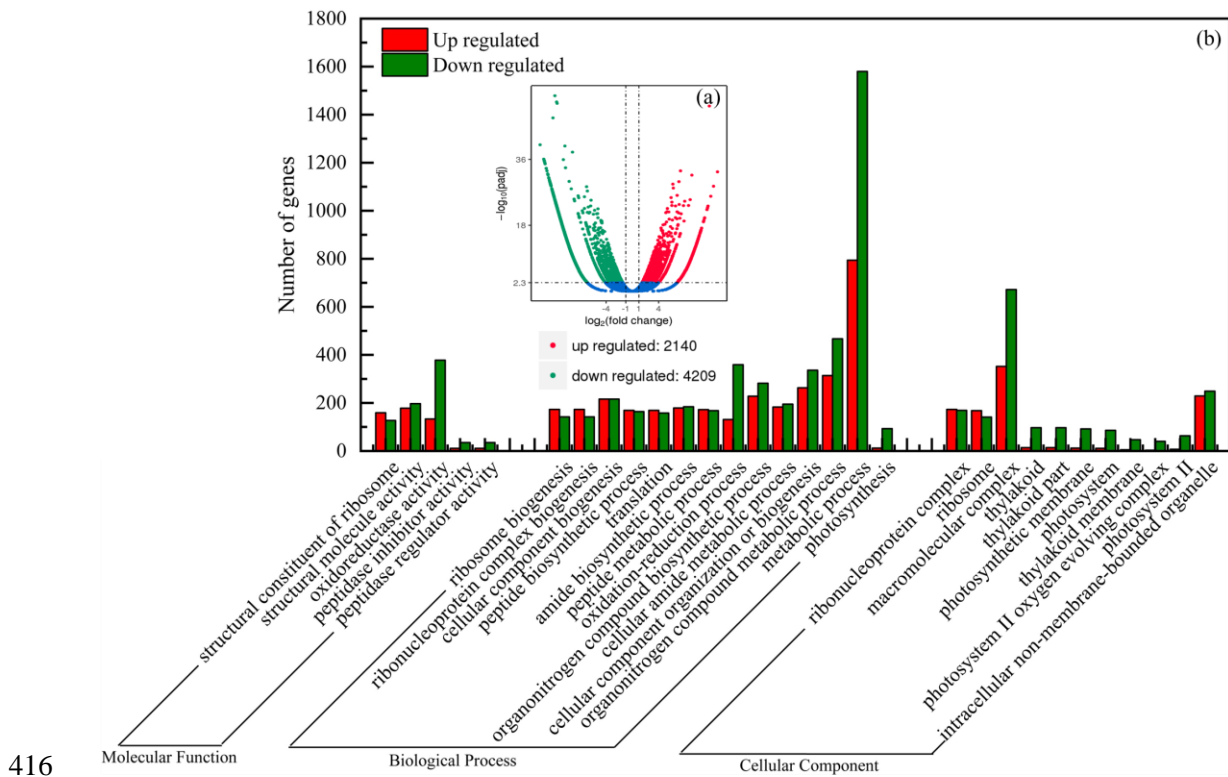
390

391 **Figure 4.** (a) Gene expression changes in *Iris* plants of the H-NB group (DO = 7.52 ± 0.65  
 392 mg/L) compared with the MAB group (DO = 7.49 ± 0.56 mg/L). (b) Significantly enriched  
 393 Gene Ontology (GO) classification of differentially expressed genes ( $p < 0.05$ ).

394 In *Echinodorus*, there were significantly more downregulated (4209) than  
 395 upregulated (2140) genes in plants from the S-NB group compared to the MAB group (Fig.  
 396 5a). The submergent nature of *Echinodorus*, meaning that it was completely immersed in  
 397 the bulk nanobubble water, may lead to more oxygen stress than in *Iris* and the subsequent  
 398 breakdown of the antioxidant system. Thus, 131 upregulated unigenes and 359  
 399 downregulated unigenes were found under the ‘oxidation-reduction process’ heading  
 400 (Table S2). In addition, most genes related to photosynthesis, such as ‘thylakoid’,  
 401 ‘thylakoid membrane’, ‘photosystem’ and ‘photosynthetic membrane’, were downregulated  
 402 (Fig. 5b). The chloroplast structure was severely damaged and chlorophyll content  
 403 significantly decreased at high nanobubble concentrations (Fig. 2d and Fig. 5b), which is

404 also consistent with hyperoxia stress. It has been documented that the rate of  
 405 photosynthesis can be inhibited by high oxygen concentrations.<sup>37-39</sup> Oxygen is a  
 406 competitive inhibitor of carbon dioxide fixation and can result in a significant decrease (up  
 407 to 60%) in photosynthetic efficiency and photosynthetic output.<sup>40</sup> Therefore, genes with the  
 408 ‘metabolic process’ term were downregulated, in accordance with a reduction in plant  
 409 physiological activity. In our previous experiments, the growth of *Echinodorus* was  
 410 significantly inhibited (25%) after 60 days cultivation at a high nanobubble concentration.<sup>22</sup>

411 In summary, RNA sequencing analysis shows that the ability to bind, transfer and  
 412 reduce oxygen and the stress resistance capacity in *Iris* were enhanced by nanobubble  
 413 treatment compared with macrobubble treatment at a similar DO level. However, the  
 414 antioxidant system of *Echinodorus* collapsed and both photosynthesis and general  
 415 metabolic processes were inhibited.



417 **Figure 5.** (a) Gene expression changes of *Echinodorus* in the S-NB group (DO = 7.23 ±  
418 0.19 mg/L) compared with the MAB group (DO = 7.21 ± 0.19 mg/L). (b) Significantly  
419 enriched Gene Ontology (GO) classification of differentially expressed genes ( $p < 0.05$ ).

### 420 **3.3.3 Plant hormone generation**

421 Diverse aspects of plant growth and development are controlled by the plant hormone  
422 network, which allows plants to adapt and survive in highly dynamic natural environments,  
423 including the change of the oxygen level.<sup>41</sup> At similar DO levels in the MAB and  
424 nanobubble groups, the 3-indoleacetic acid (IAA) contents in both plant species were  
425 significantly higher in nanobubble treatment groups (M-NB, H-NB and S-NB) than in the  
426 MAB group. Moreover, the IAA content increased with increasing nanobubble  
427 concentration from 31.25 ng/g (MAB group) to 84.63 ng/g (S-NB group) for *Iris*, and 1.04  
428 ng/g (MAB group) to 1.55 ng/g (S-NB group) for *Echinodorus* (Table 3). IAA can promote  
429 root initiation and induces both growth of pre-existing roots and adventitious root  
430 formation.<sup>42</sup> Therefore, the alteration in the plant root architecture was probably achieved  
431 largely through the high levels of IAA (Fig. 2b, Fig. S3),<sup>43</sup> which thereby promoted an  
432 increase in biomass (Fig. 2a). In addition, the chlorophyll degradation (photosynthesis  
433 damage) we observed may also be related to the increased IAA levels in *Echinodorus* (Fig.  
434 2d and Fig. 5b). This is supported by a previous study, which showed that the chloroplast  
435 membrane system was less developed and the chlorophyll content was lower in wheat  
436 coleoptiles treated with IAA.<sup>44</sup> Endogenous ROS generation in plants mainly results from  
437 side-reactions of the photosynthesis process,<sup>45</sup> and therefore IAA is likely to reduce ROS  
438 generation in the S-NB group by remodelling the photosynthetic apparatus and thereby  
439 minimizing oxidative damage (Fig. 2d and Fig. 5).<sup>41</sup>

440 Moreover, the levels of salicylic acid (SA), jasmonic acid (JA) and jasmonic acid-  
 441 isoleucine (JA-ILE), which play important roles in plant responses to a wide range of biotic  
 442 and abiotic stresses,<sup>46</sup> also significantly increased in the nanobubble groups (Table 3). SA  
 443 content reached the highest levels in the S-NB group in both plant species, while JA and  
 444 JA-ILE content first increased with increasing nanobubble concentration, and then  
 445 decreased in the S-NB group. These elevated hormone levels further demonstrate that  
 446 nanobubbles cause hyperoxia stress in plants, which trigger plant defences and promote  
 447 physiological adaptation.

448 The results described so far indicate that exposure to nanobubbles can alter redox  
 449 homeostasis, gene expression and hormone generation in plants. Previous studies show that  
 450 the ROS signalling pathway consists of an elaborate network that exhibits frequent  
 451 crosstalk with gene<sup>47</sup> and hormone<sup>41</sup> pathways. The endogenous ROS induced by  
 452 nanobubbles can thus regulate the growth and development of plants in concert with T-  
 453 AOC, genes and plant hormones.

454 **Table 3**

455 Hormone changes in plants of different groups with similar DO levels.

		Phytohormone (ng/g)			
		IAA	SA	JA	JA-ILE
<i>Iris</i> root	MAB	31.25 ± 2.40 <sup>d</sup>	55.21 ± 2.74 <sup>b</sup>	1.73 ± 0.08 <sup>d</sup>	1.40 ± 0.05 <sup>c</sup>
	M-NB	44.73 ± 1.90 <sup>c</sup>	58.37 ± 3.87 <sup>b</sup>	6.35 ± 0.35 <sup>b</sup>	2.06 ± 0.21 <sup>b</sup>
	H-NB	56.18 ± 2.47 <sup>b</sup>	52.47 ± 4.47 <sup>b</sup>	8.44 ± 0.42 <sup>a</sup>	3.41 ± 0.34 <sup>a</sup>
	S-NB	84.63 ± 2.64 <sup>a</sup>	87.34 ± 2.56 <sup>a</sup>	3.90 ± 0.12 <sup>c</sup>	3.15 ± 0.31 <sup>a</sup>
<i>Echinodorus</i> leaf	MAB	1.04 ± 0.08 <sup>c</sup>	/	5.10 ± 0.39 <sup>c</sup>	2.54 ± 0.26 <sup>a</sup>
	M-NB	1.12 ± 0.15 <sup>c</sup>	/	9.90 ± 2.89 <sup>b</sup>	3.01 ± 0.62 <sup>a</sup>
	H-NB	1.39 ± 0.02 <sup>b</sup>	2.96 ± 0.09 <sup>b</sup>	16.61 ± 1.14 <sup>a</sup>	2.39 ± 0.16 <sup>a</sup>
	S-NB	1.55 ± 0.04 <sup>a</sup>	3.50 ± 0.17 <sup>a</sup>	2.43 ± 0.31 <sup>d</sup>	0.98 ± 0.28 <sup>b</sup>

456 IAA, SA, JA, JA-ILE represent 3-indoleacetic acid, salicylic acid, jasmonic acid, jasmonic  
 457 acid-isoleucine, respectively. Error bars indicate standard deviations. The different letters  
 458 indicate significant differences ( $p < 0.05$ ) compared with other groups of the same plant.



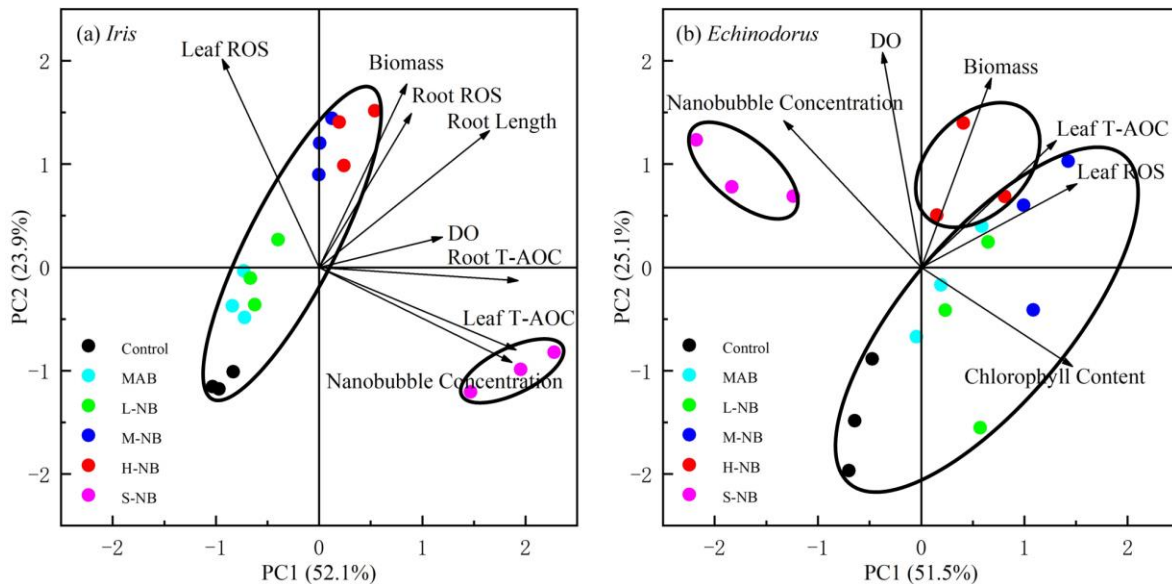
### 459 **3.4 Overall mechanisms**

460 The principal component analysis (PCA) was used to visualise the effect of  
461 nanobubble concentrations on plant growth responses (Fig. 6a and b). The growth medium  
462 conditions (DO and nanobubble concentrations), plant morphology parameters (biomass  
463 growth ratio and root length for *Iris*, biomass growth ratio and chlorophyll content for  
464 *Echinodorus*), and plant physiology parameters (ROS and T-AOC for *Iris* leaf and root, and  
465 for *Echinodorus* leaf) were included in the analysis.

466 For both species (Fig. 6a and b), the factor of nanobubble concentration clearly drives  
467 the S-NB groups away from other groups in the coordinate. Closer examination of the  
468 *Echinodorus* data (Fig. 6b) shows that the H-NB groups also follow the direction of the  
469 nanobubble concentration factor, causing them to differentiate from other groups. This  
470 agrees with our results showing that the nanobubble concentration thresholds that  
471 significantly influence the growth of *Iris* and *Echinodorus* are likely  $3.45 \times 10^7$  particles/mL  
472 (H-NB group) and  $1.23 \times 10^7$  particles/mL (M-NB group), respectively: below the threshold,  
473 increasing nanobubble concentration can significantly improve plant growth (Fig. 2). The  
474 patterns of other groups cluster together in a right-up direction for both species (Fig. 6) as  
475 the nanobubble concentration increases (from control to MAB and to H-NB groups).  
476 Biomass growth ratio, ROS (for *Iris* root or *Echinodorus* leaf), root length (*Iris*) and  
477 chlorophyll content (*Echinodorus*) are the main factors contributing to the right-up  
478 direction. Endogenous ROS appears to be a major factor affecting plant biomass (Fig. 6),  
479 which is consistent with the improvement in plant performance that can occur with  
480 appropriate levels of ROS. In addition, the increase in nanobubble concentration  
481 contributed to the T-AOC content increase in *Iris* leaf and root (Fig. 6a), but chlorophyll

482 content changed in the opposite direction, i.e. decreased, with nanobubble concentration in  
483 *Echinodorus* (Fig. 6b).

484 The emergent species clearly has a higher tolerance of nanobubbles. Although the DO  
485 levels in all groups were similar, the enhanced oxygen delivery in water resulting from the  
486 stability and high gas density of nanobubbles<sup>48,49</sup> may promote plant aerobic respiration and  
487 the generation of endogenous ROS in plants, resulting in the increase of antioxidant  
488 capacity in plants and superior plant growth. However, when the nanobubble concentration  
489 exceeds the threshold, the toxicity of oxygen will become dominant and induce hyperoxia  
490 stress, particularly in submergent plants, which may result in collapse of the antioxidant  
491 system and the inhibition of photosynthesis. The physiological responses of the aquatic  
492 plants may also be caused by the oxidation substances, such as the free radicals released  
493 from the nanobubble. Further studies are needed to investigate the free radicals and their  
494 interactions with the relevant hyperoxia stress of aquatic plants.



495  
496 **Figure 6.** Principal component analysis (PCA) of results from the morphological and  
497 physiological responses of *Iris* (a) and *Echinodorus* (b) in the various groups. The points

498 from different experimental groups in the same circle represent their clear differences with  
499 the data points in other circles during the PCA analysis.

500 Bulk nanobubble and interfacial nanobubble technology have both been used for the  
501 restoration of eutrophic and black-odour water in recent years. As a sustainable and  
502 efficient technology, nanobubble technology offers many advantages with respect to  
503 internal nutrient loading control, HAB removal and water quality improvement. Generally,  
504 using a higher concentration of nanobubbles or pure oxygen nanobubbles results in a  
505 greater improvement in water quality. However, natural water restoration is a systematic  
506 process, of which the restoration of aquatic vegetation following an improvement in the  
507 water quality is an important part. Our results demonstrate that nanobubbles can promote  
508 plant aerobic respiration and the generation of endogenous ROS in plants, which improve  
509 plant growth. The energy consumption ( $31.25 \text{ W/m}^3$ ) in the M-NB group was one fifth of  
510 that ( $150 \text{ W/m}^3$ ) in the MAB group (Table 1), but exhibited a better performance in  
511 promoting plant growth. Nevertheless, extremely high nanobubble concentrations induce  
512 hyperoxia stress and inhibit plant physiological activity, such as oxidation-reduction,  
513 photosynthesis and metabolic processes. Notably, the identified thresholds for the aquatic  
514 plants were confirmed under experimental conditions with the homogenised nanobubble  
515 concentration. The nanobubble concentrations would vary in different areas of the natural  
516 waters, which need to be considered when using the current finding to guide the practical  
517 application.

#### 518 **4. Conclusion**

519 This study investigated the morphological and physiological response of both  
520 emergent (*Iris*) and submergent (*Echinodorus*) aquatic plants during the later stage of the

521 nanobubble-induced water restoration process. This study demonstrated the nanobubble  
522 concentration thresholds for the switch from growth promotion to growth inhibition are  
523  $3.45 \times 10^7$  and  $1.23 \times 10^7$  particles/mL for *Iris* and *Echinodorus*, respectively. The growth of  
524 both aquatic plants was promoted, under this threshold, due to the improved aerobic  
525 respiration and the generation of ROS in plants. However, excessed nanobubbles could  
526 induce hyperoxia stress, affect the expression of genes and the generation of relevant  
527 hormones. Therefore, using a higher concentration of nanobubbles could achieve the  
528 effective water quality improvement, however, appropriate concentrations of nanobubble  
529 (approximate  $10^7$  particles/mL) should be controlled to facilitate the aquatic vegetation  
530 growth towards throughout eutrophication management and water restoration. Meanwhile,  
531 the potentially different thresholds for other aquatic vegetation species should be further  
532 studied.

### 533 **ASSOCIATED CONTENT**

534 The Supporting Information is available free of charge at <http://pubs.acs.org>.

535 Information about the changes in DO level and pH during cultivation of *Iris* and  
536 *Echinodorus*, the appearance of *Iris* root and the significantly enriched Gene Ontology (GO)  
537 classification of DEGs in the two plants (PDF).

### 538 **AUTHOR INFORMATION**

#### 539 **Corresponding Authors**

540 **Pan Li** – *State Key Laboratory of Control and Resource Reuse, School of Environmental*  
541 *Science and Engineering, Tongji University, 1239 Siping Road, Shanghai, PR China;*  
542 *orcid.org/0000-0002-5192-8509; E-mail: [lipan@tongji.edu.cn](mailto:lipan@tongji.edu.cn)*

543 **Gang Pan** – *Integrated Water-Energy-Food Facility (iWEF), School of Animal, Rural, and*  
544 *Environmental Sciences, Nottingham Trent University, Nottinghamshire NG25 0QF, UK;*  
545 *orcid.org/0000-0003-0920-3018; E-mail: [gang.pan@ntu.ac.uk](mailto:gang.pan@ntu.ac.uk)*

#### 546 **Authors**

547 **Shuo Wang** – *School of Environmental Science and Engineering, Tongji University, 1239*  
548 *Siping Road, Shanghai, PR China; orcid.org/0000-0002-2072-2962*

549 **Yunsi Liu** – *School of Environmental Science and Engineering, Tongji University, 1239*  
550 *Siping Road, Shanghai, PR China; orcid.org/0000-0002-6315-7705*

551 **Tao Lyu** – *Cranfield Water Science Institute, Cranfield University, College Road,*  
552 *Cranfield, Bedfordshire, MK43 0AL, UK; orcid.org/0000-0001-5162-8103*

#### 553 **Notes**

554 The authors declare no competing financial interest.

#### 555 **Acknowledgements**

556 This work was supported in part by The National Major Science and Technology Project of  
557 China (2017ZX07201002) and partially by a scholarship from the China Scholarship  
558 Council (CSC).

#### 559 **Reference**

- 560 (1) Agarwal, A.; Ng, W. J.; Liu, Y. Principle and Applications of Microbubble and  
561 Nanobubble Technology for Water Treatment. *Chemosphere* **2011**, *84* (9), 1175–  
562 1180.
- 563 (2) Takahashi, M.; Chiba, K.; Li, P. Free-Radical Generation from Collapsing  
564 Microbubbles in the Absence of a Dynamic Stimulus. *J. Phys. Chem. B* **2007**, *111*  
565 (6), 1343–1347.

- 566 (3) Li, P.; Song, Y.; Yu, S. Removal of *Microcystis Aeruginosa* Using Hydrodynamic  
567 Cavitation: Performance and Mechanisms. *Water Res.* **2014**, *62*, 241–248.
- 568 (4) Sun, Y.; Wang, S.; Niu, J. Microbial Community Evolution of Black and Stinking  
569 Rivers during in Situ Remediation through Micro-Nano Bubble and Submerged  
570 Resin Floating Bed Technology. *Bioresour. Technol.* **2018**, *258*, 187–194.
- 571 (5) Wu, Y.; Lin, H.; Yin, W.; Shao, S.; Lv, S.; Hu, Y. Water Quality and Microbial  
572 Community Changes in an Urban River after Micro-Nano Bubble Technology in  
573 Situ Treatment. *Water* **2019**, *11* (1), 66.
- 574 (6) Zhang, H. Combating Hypoxia/Anoxia at Sediment-Water Interfaces: A Preliminary  
575 Study of Oxygen Nanobubble Modified Clay Materials. *Sci. Total Environ.* **2018**, *11*.
- 576 (7) Shi, W.; Pan, G.; Chen, Q.; Song, L.; Zhu, L.; Ji, X. Hypoxia Remediation and  
577 Methane Emission Manipulation Using Surface Oxygen Nanobubbles. *Environ. Sci.*  
578 *Technol.* **2018**, *52* (15), 8712–8717.
- 579 (8) SOLitude. Oxygenate Your Waterbody With Nanobubble Aeration  
580 <https://www.solitudelakemanagement.com/ultra-fine-nanobubble-technology>. **2019**,  
581 (accessed Jun 16, 2020).
- 582 (9) Gunther, T. Lakes can breathe again: Introducing pure oxygen nanobubble solution  
583 [https://smartwatermagazine.com/news/lg-sonic/lakes-can-breathe-again-introducing-](https://smartwatermagazine.com/news/lg-sonic/lakes-can-breathe-again-introducing-pure-oxygen-nanobubble-solution)  
584 [pure-oxygen-nanobubble-solution](https://smartwatermagazine.com/news/lg-sonic/lakes-can-breathe-again-introducing-pure-oxygen-nanobubble-solution). **2019**, (accessed Jun 16, 2020).
- 585 (10) Zhang, Y.; Jeppesen, E.; Liu, X.; Qin, B.; Shi, K.; Zhou, Y.; Thomaz, S. M.; Deng, J.  
586 Global Loss of Aquatic Vegetation in Lakes. *Earth-Sci. Rev.* **2017**, *173*, 259–265.
- 587 (11) Dat, J. F.; Folzer, H.; Parent, C.; Badot, P.-M.; Capelli, N. Hypoxia Stress: Current  
588 Understanding and Perspectives. *Floriculture, Ornamental and Plant Biotechnology:*  
589 *Advances and Topical Issues*, Global Science Books, 2006, pp.664-674.

- 590 (12) Ahmed, A.; Shi, X.; Hua, L.; Manzueta, L.; Qing, W.; Marhaba, T.; Zhang, W.  
591 Influences of Air, Oxygen, Nitrogen, and Carbon Dioxide Nanobubbles on Seed  
592 Germination and Plant Growth. *J. Agric. Food Chem.* **2018**, *66*.
- 593 (13) Park, J.-S.; Kurata, K. Application of Microbubbles to Hydroponics Solution  
594 Promotes Lettuce Growth. *HortTechnology* **2009**, 212–215.
- 595 (14) Ikeura, H.; Tsukada, K.; Tamaki, M. Effect of Microbubbles in Deep Flow  
596 Hydroponic Culture on Spinach Growth. *J. Plant Nutr.* **2017**, *40* (16), 2358–2364.
- 597 (15) Wu, Y.; Lyu, T.; Yue, B.; Tonoli, E.; Verderio, E. A. M.; Ma, Y.; Pan, G.  
598 Enhancement of Tomato Plant Growth and Productivity in Organic Farming by Agri-  
599 Nanotechnology Using Nanobubble Oxygenation. *J. Agric. Food Chem.* **2019**, *67* (39),  
600 10823–10831.
- 601 (16) Liu, S.; Oshita, S.; Kawabata, S.; Makino, Y.; Yoshimoto, T. Identification of ROS  
602 Produced by Nanobubbles and Their Positive and Negative Effects on Vegetable  
603 Seed Germination. *Langmuir* **2016**, *32* (43), 11295–11302.
- 604 (17) Liu, S.; Oshita, S.; Makino, Y.; Wang, Q.; Kawagoe, Y.; Uchida, T. Oxidative  
605 Capacity of Nanobubbles and Its Effect on Seed Germination. *ACS Sustain. Chem.*  
606 *Eng.* **2016**, *4* (3), 1347–1353.
- 607 (18) Mittler, R. ROS Are Good. *Trends Plant Sci.* **2017**, *22* (1), 11–19.
- 608 (19) Morimoto, H.; Iwata, K.; Ogonuki, N.; Inoue, K.; Atsuo, O.; Kanatsu-Shinohara, M.;  
609 Morimoto, T.; Yabe-Nishimura, C.; Shinohara, T. ROS Are Required for Mouse  
610 Spermatogonial Stem Cell Self-Renewal. *Cell Stem Cell.* **2013**, *12* (6), 774–786.
- 611 (20) Ikeura, H.; Takahashi, H.; Kobayashi, F.; Sato, M.; Tamaki, M. Effect of Different  
612 Microbubble Generation Methods on Growth of Japanese Mustard Spinach. *J. Plant*  
613 *Nutr.* **2017**, *40* (1), 115–127.

- 614 (21) Ikeura, H.; Takahashi, H.; Kobayashi, F.; Sato, M.; Tamaki, M. Effects of  
615 Microbubble Generation Methods and Dissolved Oxygen Concentrations on Growth  
616 of Japanese Mustard Spinach in Hydroponic Culture. *J. Hortic. Sci. Biotechnol.* **2018**,  
617 *93* (5), 483–490.
- 618 (22) Wang, S.; Liu, Y.; Li, P.; Wang, Y.; Yang, J.; Zhang, W. Micro-Nanobubble  
619 Aeration Promotes Senescence of Submerged Macrophytes with Low Total  
620 Antioxidant Capacity in Urban Landscape Water. *Environ. Sci. Water Res. Technol.*  
621 **2020**, *6* (3), 523–531.
- 622 (23) Das, K.; Samanta, L.; Chainy, G. B. N. A Modified Spectrophotometric Assay of  
623 Superoxide Dismutase Using Nitrite Formation by Superoxide Radicals. *IJBB*  
624 *Vol373*. **2000**, *6*.
- 625 (24) Schneider, K.; Schlegel, H. G. Production of Superoxide Radicals by Soluble  
626 Hydrogenase from *Alcaligenes Eutrophus* H16. *Biochem. J.* **1981**, *193* (1), 99–107.
- 627 (25) Young, M. D.; Wakefield, M. J.; Smyth, G. K.; Oshlack, A. Gene Ontology Analysis  
628 for RNA-Seq: Accounting for Selection Bias. *Genome Biol.* **2010**, *11* (2), R14.
- 629 (26) Robinson, M. D.; McCarthy, D. J.; Smyth, G. K. EdgeR: A Bioconductor Package  
630 for Differential Expression Analysis of Digital Gene Expression Data.  
631 *Bioinformatics.* **2010**, *26* (1), 139–140.
- 632 (27) Storey, J. D.; Tibshirani, R. Statistical Significance for Genomewide Studies. *Proc.*  
633 *Natl. Acad. Sci. U. S. A.* **2003**, *100* (16), 9440–9445.
- 634 (28) Tan, B. H.; An, H.; Ohl, C.-D. How Bulk Nanobubbles Might Survive. *Phys. Rev.*  
635 *Lett.* **2020**, *124* (13), 134503.

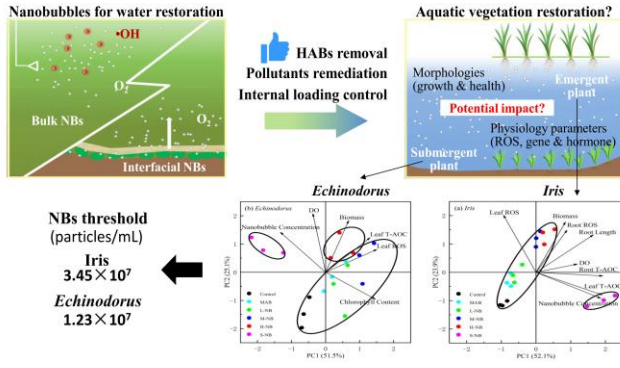


- 636 (29) Chen, C.; Li, J.; Zhang, X. The Existence and Stability of Bulk Nanobubbles: A  
637 Long-Standing Dispute on the Experimentally Observed Mesoscopic  
638 Inhomogeneities in Aqueous Solutions. *Commun. Theor. Phys.* **2020**, *72* (3), 037601.
- 639 (30) Zhang, X. H.; Maeda, N.; Craig, V. S. J. Physical Properties of Nanobubbles on  
640 Hydrophobic Surfaces in Water and Aqueous Solutions. *Langmuir* **2006**, *22* (11),  
641 5025–5035.
- 642 (31) Soffer, H.; Burger, D. W. Effects of Dissolved Oxygen Concentrations in Aero-  
643 Hydroponics on the Formation and Growth of Adventitious Roots. **1998**, *5*.
- 644 (32) Suyantohadi, A.; Kyoren, T.; Hariadi, M.; Purnomo, M. H.; Morimoto, T. Effect of  
645 High Concentrated Dissolved Oxygen on the Plant Growth in a Deep Hydroponic  
646 Culture under a Low Temperature. *IFAC Proc. Vol.* **2010**, *43* (26), 251–255.
- 647 (33) Kurashina, Y.; Yamashita, T.; Kurabayashi, S.; Takemura, K.; Ando, K. Growth  
648 Control of Leaf Lettuce with Exposure to Underwater Ultrasound and Dissolved  
649 Oxygen Supersaturation. *Ultrason. Sonochem.* **2019**, *51*, 292–297.
- 650 (34) Bartosz, G. Oxidative stress in plants. *Acta Physiol Plant.* **1997**, *19*, 47–64.
- 651 (35) Simontacchi, M.; Caro, A.; Puntarulo, S. Oxygen-Dependent Increase of  
652 Antioxidants in Soybean Embryonic Axes. *Int. J. Biochem. Cell Biol.* **1995**, *27* (11),  
653 1221–1229.
- 654 (36) Hardison, R. C. A Brief History of Hemoglobins: Plant, Animal, Protist, and Bacteria.  
655 *Proc. Natl. Acad. Sci. U. S. A.* **1996**, *93* (12), 5675–5679.
- 656 (37) Wroblewska, B.; Mostowska, A.; Poskuta, J. The Effect of Oxygen Concentration on  
657 Chloroplast Development, Chlorophyll Synthesis and Starch Accumulation in  
658 Etiolated Bean Seedlings upon Illumination. *Environ. Exp. Bot.* **1994**, *34* (2), 153–  
659 163.

- 660 (38) Turner, J. S.; Brittain, E. G. Oxygen as a Factor in Photosynthesis. *Biol. Rev.* **1962**,  
661 37 (1), 130–170.
- 662 (39) Zelitch, I. *Photosynthesis, Photorespiration, And Plant Productivity*; Elsevier  
663 Science, 2012.
- 664 (40) Mohr, H.; Schopfer, P. *Plant Physiology*; Springer Science & Business Media, **1995**.
- 665 (41) Tognetti, V. B.; Mühlenbock, P.; Breusegem, F. V. Stress Homeostasis – the Redox  
666 and Auxin Perspective. *Plant Cell Environ.* **2012**, 35 (2), 321–333.
- 667 (42) Walker, P. M. B. *Chambers Dictionary of Science and Technology*; London :  
668 Chambers, **1999**.
- 669 (43) Pandey, V.; Bhatt, I. D.; Nandi, S. K. Chapter 20 - Role and Regulation of Auxin  
670 Signaling in Abiotic Stress Tolerance. In *Plant Signaling Molecules*; Khan, M. I. R.,  
671 Reddy, P. S., Ferrante, A., Khan, N. A., Eds.; Woodhead Publishing, **2019**; pp 319–  
672 331.
- 673 (44) Volfová, A.; Chvojka, L.; Friedrich, A. The Effect of Kinetin and Auxin on the  
674 Chloroplast Structure and Chlorophyll Content in Wheat Coleoptiles. *Biol. Plant.*  
675 **1978**, 20 (6), 440–445.
- 676 (45) Foyer, C. H.; Noctor, G. Redox Sensing and Signalling Associated with Reactive  
677 Oxygen in Chloroplasts, Peroxisomes and Mitochondria. *Physiol. Plant.* **2003**, 119  
678 (3), 355–364.
- 679 (46) Bari, R.; Jones, J. D. G. Role of Plant Hormones in Plant Defence Responses. *Plant*  
680 *Mol. Biol.* **2009**, 69 (4), 473–488.
- 681 (47) Vandebroucke, K.; Robbens, S.; Vandepoele, K.; Inzé, D.; Van de Peer, Y.; Van  
682 Breusegem, F. Hydrogen Peroxide–Induced Gene Expression across Kingdoms: A  
683 Comparative Analysis. *Mol. Biol. Evol.* **2008**, 25 (3), 507–516.

- 684 (48) Zhou, L.; Wang, X.; Shin, H.-J.; Wang, J.; Tai, R.; Zhang, X.; Fang, H.; Xiao, W.;  
685 Wang, L.; Wang, C.; Gao, X.; Hu, J.; Zhang, L. Ultrahigh Density of Gas Molecules  
686 Confined in Surface Nanobubbles in Ambient Water. *J. Am. Chem. Soc.* **2020**, *142*  
687 (12), 5583–5593.
- 688 (49) Ghaani, M. R.; Kusalik, P. G.; English, N. J. Massive Generation of Metastable Bulk  
689 Nanobubbles in Water by External Electric Fields. *Sci. Adv.* **2020**, *6* (14), eaaz0094.

690 **Table of Contents**



691